The Characteristic Response of Whistler Mode Waves to Interplanetary Shocks

Yue, C.; Chen, L.; Bortnik, J.; Ma, Q.; Thorne, R. M.; Angelopolous, V.; Li, J.; An, X.; Zhou, C.; Kletzing, C.; Reeves, Geoffrey D.; spence, H. E.

To be published in: Journal of Geophysical Research: Space Physics

DOI to publisher's version: 10.1002/2017JA024574

The characteristic response of whistler mode waves to interplanetary shocks

Chao Yue[1, 2], Lunjin Chen[3], Jacob Bortnik[1], Qianli Ma[1,4], Richard M. Thorne[1], Vassilis Angelopoulos[5,6], Jinxing Li[1], Xin An[1], Chen Zhou[7], Craig Kletzing[8], Geoffrey D. Reeves[9,10], Harlan E. Spence[11]

1. Department of Atmospheric and Oceanic Sciences, University of California, Los Angeles, California, USA
2. University Corporation for Atmospheric Research, Boulder, CO, USA
3. Physics Department, University of Texas at Dallas, Richardson, TX
4. Center for Space Physics, Boston University, Boston, Massachusetts, USA.
5. Department of Earth, Planetary and Space Sciences, University of California, Los Angeles, California, USA
6. Institute of Geophysics and Planetary Physics, University of California, Los Angeles, California, USA
7. Department of Space Physics, School of Electronic Information, Wuhan University, Wuhan, China
8. Department of Physics and Astronomy, University of Iowa, Iowa City, Iowa, USA
9. Space Science and Applications Group, Los Alamos National Laboratory, Los Alamos, New Mexico, USA.
10. Space Sciences Division at the New Mexico Consortium, Los Alamos, New Mexico, USA.
11. Institute for the Study of Earth, Oceans, and Space, University of New Hampshire, Durham, New Hampshire, USA.

Abstract:

Magnetospheric whistler mode waves play a key role in regulating the dynamics of the electron radiation belts. Recent satellite observations indicate a significant influence of interplanetary (IP) shocks on whistler mode wave power in the inner magnetosphere. In this study, we statistically investigate the response of whistler mode chorus and plasmaspheric hiss to IP shocks based on Van Allen Probes and THEMIS satellite observations. Immediately after the IP shock arrival, chorus wave power is usually intensified, often at dawn, while plasmaspheric hiss wave power predominantly decreases near the dayside but intensifies near the nightside. We conclude that chorus wave intensification outside the plasmasphere is probably associated with the suprathermal electron flux enhancement caused by the IP shock. On the other hand, the solar wind dynamic pressure increase changes the magnetic field configuration to favor ray penetration into the nightside and promote ray refraction away from the dayside, explaining the magnetic local time (MLT) dependent responses of plasmaspheric hiss waves following IP shock arrivals.

1. Introduction

Chorus emissions are intense electromagnetic whistler mode waves with discrete elements, excited naturally in the low-density region outside the plasmapause due to cyclotron instability of energetic anisotropic electrons [*Tsurutani and Smith,* 1974; *Meredith et al.,* 2001, 2003; *Yue et al.,* 2016b; *An et al,* 2017]. They typically occur in the range 0.1–0.8 f_{ce} (f_{ce} is the equatorial electron cyclotron frequency), commonly in two distinct bands (lower and upper bands) with a gap near 0.5 f_{ce} [*Tsurutani and Smith*, 1977; *Santolík et al.,* 2003]. Previous studies have shown that nightside chorus waves are confined to within ~15° of the magnetic equator, whereas dayside chorus waves can extend to higher magnetic latitudes (MLAT) [e.g., *Li et al.,* 2009; *Bunch et al*., 2011]. Recent studies have demonstrated the important role played by chorus waves in both the loss of plasma sheet electrons and the acceleration of radiation belt relativistic electrons [e.g., *Lorentzen et al*., 2001; *Horne et a*l., 2005; *Thorne et al.,* 2005; *Chen et al.*, 2007; *Li et al.,* 2007; *Shprits et al.*, 2009; *Thorne*, 2010; *Reeves et al.,* 2013; *Thorne et al.,* 2013a; 2013b; *Ni et al.,* 2014; *Baker et al.,* 2014].

Plasmaspheric hiss waves is a structureless, broadband whistler mode emission typically observed within the high plasma density regions that surround the Earth, including the plasmasphere and plasmaspheric plumes [*Dunckel and Helliwell*, 1969; *Thorne et al.,* 1973; *Meredith et al.,* 2004; *Summers et al.,* 2008]. Plasmaspheric hiss is widely distributed in radial distance and magnetic local time (MLT); the strongest emissions typically occur near the dayside plasmasphere [*Li et al.*, 2015; *Spasojevic et al*., 2015]. Plasmaspheric hiss causes precipitation of electrons from tens of keV to a few MeV to the upper atmosphere through pitch angle scattering on time scales ranging from days to weeks [*Lyons and Thorne,* 1973; *Meredith et al.,* 2006, 2007, 2009; *Thorne et al.*, 2013b; *Ma et al.*, 2016]. Ray tracing and conjunctive satellite observations have shown that whistler mode chorus waves outside the plasmapause can propagate into the plasmasphere where it can be amplified further to form plasmaspheric hiss [*Bortnik et al.,* 2008, 2009a; 2009b; *Chen et al.,* 2012].

The whistler wave power in the inner magnetosphere may significantly change following the arrival of an interplanetary (IP) shock. *Su et al.* [2015] have reported enhanced damping and resultant disappearance of plasmaspheric hiss due to increased fluxes of superthermal electrons during an IP shock event with Van Allen Probes observations. The disappearance of plasmaspheric hiss, exohiss, and chorus waves may also be caused by increased field line inhomogeneity after the solar wind dynamic pressure decrease [*Liu et al.,* 2017], which tends to inhibit wave growth and propagation.

Only few studies of the whistler wave amplification/suppression have been done in the past due to the scarcity of such events and the fortuitous presence of near-Earth satellites at the right locations to observe the waves. It is thus presently unclear what the effects of IP shocks on whistler mode waves are as function of MLT, and what controls the wave amplification or damping during the passage of IP shocks. Such knowledge is critical in order to further understand the origin of particle acceleration or precipitation during the passage of IP shocks. Towards that goal, we surveyed 86 forward IP shock (dynamic pressure abrupt increases following IP shock arrival) events from 2010 to 2016 based on the upstream Advanced Composition Explorer (ACE) and Wind satellite observations (the shock list can be found here: https://www.cfa.harvard.edu/shocks/) to investigate the effects of IP shocks on the whistler mode waves, including plasmaspheric hiss and whistler mode chorus waves, using Van Allen Probes (A and B) and Time

History of Events and Macroscale Interactions during Substorms (THEMIS) (A, D and E) spacecraft observations, and report the different responses of chorus wave and plasmaspheric hiss at different MLTs to the IP shocks. We also employed the two near-Earth ARTEMIS P1 and P2 satellites (also known as THEMIS B and C), when available, as high-fidelity upstream monitors.

2. Data and Instrumentation

Van Allen Probes (otherwise known as the Radiation Belt Storm Probes, RBSP, mission) consists of two identically instrumented, near-equatorial (10^o inclination) spacecraft in operation since 30 August 2012 [*Mauk et al.,* 2013]. Both satellites are equipped with comprehensive suites of particles and fields instruments. Here we perform our survey by using the electric and magnetic power spectral densities from the High-Frequency Receiver (HFR) and the Waveform Receiver (WFR) of the Electric and Magnetic Field Instrument Suite and Integrated Science instrument (EMFISIS) [*Kletzing et al.*, 2013]. The suprathermal (hundreds of eV to tens of keV) electron fluxes are observed by the Helium Oxygen Proton Electron Mass Spectrometer (HOPE) [*Funsten et al.,* 2013] of the Energetic Particle, Composition, and Thermal Plasma (ECT) Suite [*Spence et al.,* 2013]. Background electron density is derived from the upper hybrid resonance frequency measured by EMFISIS or from the spacecraft potential measured by the Electric Field and Waves (EFW) instrument [*Wygant et al.,* 2013].

THEMIS consists of five identically instrumented satellites designed to study energy releases during magnetospheric substorms [*Angelopoulos et al.,* 2008]. The wave magnetic power spectral density is obtained from the Search Coil Magnetometer (SCM) [*Le Contel et al*., 2008]. Suprathermal electron fluxes, ion density, and flow velocity are obtained from the Electrostatic Analyzer (ESA) [*McFadden et al.,* 2008]. The magnetic field is measured by the Flux Gate Magnetometer (FGM) [*Auster et al.,* 2008]. Electron density is derived from the spacecraft potential, measured by the Electric Field Instrument (EFI) [*Bonnell et al.,* 2008] and ESA.

We investigate the wave power distribution of whistler mode waves during each of the 86 IP shocks. Seventy events were observed by Van Allen Probes and sixty by THEMIS, fewer due to THEMIS' higher apogee (~12R_E) causing those spacecraft to be located often outside the magnetopause after impact of the IP shock and also due to the ~50% duty cycle of high-resolution fast survey data due to telemetry limitations. The background electron density and/or upper hybrid resonance frequency are used to identify satellite location with respect to the plasmapause [e.g., *Meredith et al.,* 2004]. Plasmaspheric hiss waves are identified typically inside the plasmasphere, and chorus waves typically in the plasma trough. Each single spacecraft observation around any of the IP shocks is counted as one event. There are 123 events where spacecraft are inside the plasmasphere and 151 events where spacecraft are in plasma trough. Using 10^{-14} $(V/m)^2/Hz$ and 10^{-9} $(nT)^2/Hz$ as the lowest power thresholds for electric and magnetic power densities, respectively, we find 43 (35%) plasmaspheric hiss reduction/disappearance events, 36 (29%) plasmaspheric hiss excitation/intensification events and 62 (41%) chorus wave excitation/intensification events in response to the IP shocks.

3. Results

3.1. Case study

Figure 1 shows a representative response of whistler mode waves following an IP shock, at 16:53 UT on 7 June 2014. Figure 1a shows the solar wind magnetic field magnitude, x-component of solar wind velocity in GSE coordinate, ion number density and dynamic pressure at THEMIS-C (ARTEMIS-P2) located at (-21.2, 57.5, -1.7) R_E, outside the magnetopause. It observed the IP shock at 16:57 UT, as a total magnetic field (black curve) increase from 5 to ~15 nT, a solar wind velocity (red curve) increase (-300 to -400 km/s), ion number density increase (5 to 15 cm^{-3}), and dynamic pressure rise (1 to 4 nPa). In response, the AE and symH indices increased abruptly around 16:53 UT from 100 to >300 nT and from -5 to +25 nT, respectively (Figure 1b).

Figures 1c and 1d show the HFR-measured electric (top panels) and the WFR-measured electric and magnetic power spectral densities (2nd and 3rd panels), and the electron omni-directional energy flux from 100 eV to 20 keV (bottom panels) on board Van Allen Probe A and B, respectively. Vertical dashed lines mark the IP shock arrival (16:53 UT). The upper hybrid frequencies (positively correlated with the background electron density [*Kurth et al.,* 2014]) observed by HFR are around 20 kHz and >100 kHz in Figures 1c and 1d respectively, indicating the locations of Van Allen Probe A being outside and B being inside the plasmasphere. After the shock arrival, Van Allen Probe A observes lower band chorus excitation/intensification for several minutes. The simultaneously observed suprathermal electron flux increases could be responsible for the chorus emissions [e.g., *Meredith et al.*, 2002; *Miyoshi et al.,* 2007]. On the other hand, Van Allen Probe B, inside the plasmasphere, observes the disappearance/reduction of plasmaspheric hiss for an extended period after the shock arrival, and the suprathermal electron flux also increases there.

Opposite plasmaspheric hiss response can be observed at different spacecraft located at different MLTs during a single IP shock event. Figure 2 shows an IP shock at 17:05 on 7 February 2014 (format similar to Figure 1). THEMIS-C at (-8.3, 60.7, -2.8) R_E observed an IP shock at 17:04 UT as a total magnetic field (black curve) increase (5 to ~12nT), solar wind velocity (red curve) increase (-300 to -400 km/s), ion number density increase (4 to 13 cm^{-3}), and dynamic pressure increase (1 to 3 nPa) (Figure 2a). At 07:05 UT, AE and symH abruptly increased (0 to >150 nT and -5 to +20 nT, respectively) indicating the arrival of the shock arrival. Shortly thereafter, THEMIS-D, at L=8.4 at dusk, observed newly excited chorus waves (Figure 2b), while Van Allen Probes A and B, both inside the plasmasphere, observed hiss intensification at dusk (Figure 2c) and hiss disappearance/reduction at dawn (Figure 2d), respectively. The suprathermal electron energy flux of 0.3 to 1 keV (Figure 2d) shows obvious increase following the IP shock arrival.

3.2. Statistical results

The two representative observations in Figures 1 and 2 indicate that the chorus waves and plasmaspheric hiss can exhibit dramatically different responses to IP shocks, at different locations. In order to understand the characteristics of these whistler mode waves and look for patterns on a global scale, we have conducted a statistical survey by investigating the wave power variations during each of the 86 IP shock events we have identified. Figure 3 shows the statistical distributions of the whistler mode chorus and plasmaspheric hiss wave responses to IP shocks observed by the Van Allen Probes and THEMIS.

Van Allen Probes (cross signs) and THEMIS (diamond signs) locations at the time of IP shock arrival are shown in Figure 3a, together with the corresponding whistler wave response (color-coded). Figures 3b and 3c show whistler event distributions as function of MLTs and MLAT, respectively. Blue color represents hiss wave power reduction/disappearance; Red color represents hiss wave power intensification/excitation; Black represents chorus wave intensification/excitation. As seen in the figure, there was only intensification and no evidence of chorus wave reduction from our IP shock event list (we only investigate the forward IP shock events in association with solar wind dynamic pressure increase).

Chorus wave amplifications are mostly observed at higher L shells and outside the plasmasphere (Figure 3a), with a peak in MLT at the post-midnight to dawn sector (Figure 3b), where presumably electron injections provide the free energy source. Meanwhile, the plasmaspheric hiss wave disappearance/reduction occurs mostly on the dayside, while hiss intensification events occur at all local times except for the noon sector following the IP shock arrival. The immediate reduction/disappearance of plasmaspheric hiss following the IP shock arrival, demonstrates that hiss damping rates should be significantly increased, such that hiss wave lifetimes is comparable to the short time scale of the shock impact (~1 min). Although more wave events were observed at lower latitude ranges (due to the spacecraft trajectory), no clear latitude dependence of the wave response is found in our survey.

4. Discussion

When an IP shock impinges upon the Earth's magnetosphere, the magnetic field intensity due to the solar wind dynamic pressure increase, and the dayside magnetic field configuration becomes more compressed while the nightside magnetic field becomes more stretched [e.g., *Wang et al*., 2009; *Yue et al.,* 2009; 2011a]. Meanwhile, the thermal plasma is adiabatically heated mainly in the perpendicular direction resulting in an increase in the electron anisotropy. Subsequently, geomagnetic activity is broadly enhanced, which includes the appearance of many wave phenomena and substorm injections [e.g., *Yue et al.,* 2010; 2011b; 2013; 2016a]. Previously *Zhou et al.* [2015] have shown that chorus waves at the dayside magnetosphere are excited after the IP shock arrival. The IP shock impinging on the magnetosphere leads to a more homogeneous background magnetic field configurations in the near-equatorial dayside magnetosphere and therefore, lower the threshold of nonlinear chorus wave growth, favoring chorus wave generation [*Tao et al.,* 2014; *Keika et al.,* 2012]. This is supported by the observational evidence that a decrease of solar wind dynamic pressure causes an increase of the threshold for chorus wave excitation, and thus results in disappearance of plasmaspheric hiss and exohiss [*Liu et al*., 2017].

In this study, we have found that chorus waves intensified both on the dayside and the nightside after the IP shock arrival. We have also investigated the IP shock list by *Zhou et al.* [2015], and found that there were in fact, many events associated with chorus excitation/intensification on the nightside or at near Earth dayside region which were not originally detected. However, the authors claim that these chorus excitation/intensification events are not associated with magnetic field topology change which is the focus of their paper (private communication). Given the fact that chorus wave is excited/intensified following IP shock arrival at all MLTs, it is reasonable to expect that in addition to the background magnetic field geometry change, another important factor that causes chorus wave excitation/intensification is the enhanced flux (and anisotropy) of suprathermal electrons produced by IP shocks. We have checked all the chorus intensification events observed by Van Allen Probes and found that about 80% of them show suprathermal electron flux (anisotropy) increase.

Considering the MLT dependence of plasmaspheric hiss reduction or intensification, the major factors that could affect hiss waves include: (1) the ability of whistler-mode waves to enter the plasmasphere from outside; (2) the length of propagation paths; (3) the chorus Landau damping rate which is determined by suprathermal electron flux level; (4) hiss Landau damping inside the plasmasphere which is usually much weaker compared with chorus wave Landau damping in the plasmatrough region. The fist factor controls accessibility of chorus waves into the plasmasphere through propagation, while the latter three factors control overall path-integrated damping before and after entering the plasmasphere. Figure 4 shows an example of ray tracing in the noon-midnight meridian plane for two different geomagnetic field configurations (Kp=1 and Kp=6) of Tsyganenko 89 (T89) magnetic field model [*Tsyganenko*, 1989]. Chorus waves of different wave normal angles (color-coded) are launched in this model with a fixed frequency 500 Hz at L=7 at the magnetic equator. The background density model adopts a modified diffusive equilibrium model with a plasmapause location at L_{pp} = 5.5. The density model parameters are similar to those of *Chen et al.* [2012]. Note that instead of using dipole magnetic field, the ray tracing code (HOTRAY [*Horne*, 1989]) is extended to a more realistic T89 model to investigate the effect of magnetic field geometry on whistler mode propagation.

Compared to the magnetic field configuration corresponding to Kp=1 (Figure 4, top), for Kp=6 the magnetic field lines are more compressed on the dayside while they are more stretched at the nightside (Figure 4, bottom). The choice of the two magnetic field configurations is intended to model the magnetic field configuration change just before (Kp=1) and just after (Kp=6) the IP shock impinging the Earth's magnetosphere. From the comparison of ray paths on the nightside for the two conditions, there are much more rays, especially those with initial wave normal closer to the parallel direction, propagating into the plasmapshere for Kp=6 than during Kp=1. This can result in the plasmaspheric hiss intensification at the nightside, after the shock arrival. We have tested different magnetic field configurations, and found that a more stretched magnetic field configuration favors the chorus wave entrance into the plasmasphere. Generally, the waves with wave normal angles between 30° to 60° have easier access into the plasmasphere [e.g., *Chen et al.*, 2012], whereas with a stretched magnetic field configuration, chorus waves with almost all wave normal angles can propagate into the plasmasphere and evolve into plasmaspheric hiss. Examination of the dayside ray paths shows no significant change in terms of the number of rays that access the plasmasphere compared to the nightside. Note that here we did not consider chorus wave Landau damping for the ray tracing result to keep the model simple and only assess the propagation effect of magnetic field configuration. However, Landau damping may play a role in reducing the wave power of chorus when propagating away from the equatorial source region, and therefore prevent chorus from evolving into the plasmasphere [e.g., *Su et al.,* 2015]. In our survey, we have observed about 50% of chorus wave events with electron parallel flux increases after the IP shock arrival, which may result in the increase of Landau damping along magnetic field line.

5. Summary

In this paper, we have performed a statistical study of whistler mode wave modifications in response to IP shocks based on data from both Van Allen Probes and THEMIS observations. 86 IP shock events were studied and we found 43 (35%) plasmaspheric hiss reduction/disappearance events, 36 (29%) hiss excitation/intensification events and 62 (41%) chorus wave excitation/intensification events from single satellite observation. Our main findings are:

1. Chorus wave power is usually intensified, with most cases occurring predominately at dawn. This is generally caused by the enhancement of suprathermal electrons produced by IP shock compressions.
2. Plasmaspheric hiss disappearance events occur predominantly on the dayside. This is probably related to the enhanced Landau damping from the observed enhancements in suprathermal electron flux as well as the slight reduction in accessibility of chorus waves into the plasmasphere due to the compressed magnetic field configuration following the IP shock arrival (based on our ray tracing result).
3. Plasmaspheric hiss intensifications occur mostly on the nightside. This can be explained by the enhanced accessibility of chorus waves, which refract into the plasmasphere due to the magnetic field stretching after the shock arrival.

On average, plasmaspheric hiss intensities are an order of magnitude larger on the dayside than on the nightside due to stronger Landau damping on the nightside, and hiss intensity increases during high solar wind dynamic pressure [*Tsurutani et al.*, 2015]. However, in this study, we have demonstrated that abrupt solar wind dynamic pressure increases cause plasmaspheric hiss disappearance on the dayside and intensification on the nightside following the changes in magnetic field configuration, which favors ray penetration into the plasmasphere on the nightside while preventing ray refraction at dayside. The MLT-dependent response of plasmaspheric hiss to IP shocks was not expected and is not well understood. The nightside ray number increases are clearly demonstrated by our ray tracing model, whereas the hiss reduction/disappearance and the chorus wave excitation/intensification right after the shock arrival still needs further detailed investigation for a more comprehensive explanation. For example, Landau damping could be another factor causing the hiss reduction/disappearance on the dayside. Since the wave power and distributions significantly vary following the IP shock arrival, our study suggests the importance of investigating the detailed wave and particle distributions in studying the local wave-particle interactions especially around the periods of IP shocks.

Acknowledgments

This work was supported by the NASA Living With a Star Jack Eddy Postdoctoral Fellowship Program, administered by the UCAR Visiting Scientist Programs. Jacob Bortnik and Lunjin Chen gratefully acknowledge support from NASA LWS grant NNX13AI61G and NASA HTIDES grant NNX16AG21G. We acknowledge use of Van Allen Probes data of the Level 3 HOPE omni-dimensional data obtained from the RBSP-ECT website (www.rbsp-ect.lanl.gov/data_pub/rbspb/hope/level3/PA/), made publicly available through NASA prime contract number NAS5-01072. We acknowledge the Van Allen Probes data from the EMFISIS instrument obtained from http://emfisis.physics.uiowa.edu/Flight/, and the THEMIS data obtained from http://themis.ssl.berkeley.edu/data/themis/. We thank the World Data Center for Geomagnetism, Kyoto for providing geomagnetic indices (http://wdc.kugi.kyoto-u.ac.jp/kp/index.html), and the Space Physics Data Facility at the NASA Goddard Space Flight Center for providing the OMNI data (ftp://spdf.gsfc.nasa.gov/pub/data/omni/omni_cdaweb/).

References:

An, X., C. Yue, J. Bortnik, V. Decyk, W. Li, and R. M. Thorne (2017), On the parameter dependence of the whistler anisotropy instability, J. Geophys. Res. Space Physics, 122, doi:10.1002/2017JA023895.

Angelopoulos, V., et al. (2008), First results from the THEMIS mission, Space Sci. Rev., 141, 453–476, doi:10.1007/s11214-008-9378-4.

Auster, H. U., et al. (2008), The THEMIS fluxgate magnetometer, Space Sci. Rev., 141, 235–264, doi:10.1007/s11214-008-9365-9.

Baker, D. N., et al. (2014), An impenetrable barrier to ultrarelativistic electrons in the Van Allen radiation belts, Nature, 515, 531–534, doi:10.1038/nature13956.

Bonnell, J. W., F. S. Mozer, G. T. Delory, A. J. Hull, R. E. Ergun, C. M. Cully, V. Angelopoulos, and P. R. Harvey (2008), The Electric Field Instrument (EFI) for THEMIS, Space Sci. Rev., 141, 303–341, doi:10.1007/s11214-008-9469-2.

Bortnik, J., R. M. Thorne, and N. P. Meredith (2008), The unexpected origin of plasmaspheric hiss from discrete chorus emissions, Nature, 452, 62–66, doi:10.1038/nature06741.

Bortnik, J., W. Li, R. M. Thorne, V. Angelopoulos, C. Cully, J. Bonnell, O. LeContel, and A. Roux (2009a), An observation linking the origin of plasmaspheric hiss to discrete chorus emissions, Science, 324, 775–778.

Bortnik, J., R. M. Thorne, and N. P. Meredith (2009b), Plasmaspheric hiss overview and relation to chorus, J. Atmos. Sol. Terr. Phys., 71, 1636–1646.

Bunch, N. L., M. Spasojevic, and Y. Y. Shprits (2011), On the latitudinal extent of chorus emissions as observed by the Polar Plasma Wave Instrument, J. Geophys. Res., 116, A04204, doi:10.1029/2010JA016181.

Chen, L., J. Bortnik, W. Li, R. M. Thorne, and R. B. Horne (2012), Modeling the properties of plasmaspheric hiss: 1. Dependence on chorus wave emission, J. Geophys. Res., 117, A05201, doi:10.1029/2011JA017201.

Chen, Y., G. D. Reeves, and R. H. W. Friedel (2007), The energization of relativistic electrons in the outer Van Allen radiation belt, Nat. Phys., 3, 614–617, doi:10.1038/nphys655.

Dunckel, N., and R. A. Helliwell (1969), Whistler mode emissions on the OGO 1 satellite, J. Geophys. Res., 74, 6371–6385, doi:10.1029/JA074i026p06371.

Funsten, H. O. et al. (2013), Helium, Oxygen, Proton, and Electron (HOPE) Mass Spectrometer for the Radiation Belt Storm Probes Mission, Space Sci Rev, 1–62, doi:10.1007/s11214-013- 9968-7.

Horne, R. B. (1989), Path-integrated growth of electrostatic waves: The generation of terrestrial myriametric radiation, J. Geophys. Res., 94(A7), 8895–8909.

Horne, R. B., et al. (2005), Wave acceleration of electrons in the Van Allen radiation belts, Nature, 437, 227–230, doi:10.1038/nature03939.

Keika, K., M. Spasojevic, W. Li, J. Bortnik, Y. Miyoshi, and V. Angelopoulos (2012), PENGUIn/AGO and THEMIS conjugate observations of whistler mode chorus waves in the dayside uniform zone under steady solar wind and quiet geomagnetic conditions, J. Geophys. Res., 117, A07212, doi:10.1029/2012JA017708.

Kennel, C. F., and H. E. Petschek (1966), Limit on stably trapped particle fluxes, J. Geophys. Res., 71(1), 1–28, doi:10.1029/JZ071i001p00001.

Kletzing, C. A., et al. (2013), The Electric and Magnetic Field Instrument Suit and Integrated Science (EMFISIS) on RBSP, Space Sci. Rev., doi:10.1007/s11214-013-9993-6.

Kurth, W. S., S. D. Pascuale, J. B. Faden, C. A. Kletzing, G. B. Hospodarsky, S. Thaller, and J. R. Wygant (2014), Electron densities inferred from plasma wave spectra obtained by the waves instrument on Van Allen Probes, J. Geophys. Res. Space Physics, 120, 904–914, doi:10.1002/2014JA020857.

Le Contel, O., et al. (2008), First results of the THEMIS Search Coil Magnetometers, Space Sci. Rev., 141, 509–34, doi:10.1007/s11214-008-9371-y.

Li, W., Y. Y. Shprits, and R. M. Thorne (2007), Dynamic evolution of energetic outer zone electrons due to wave-particle interactions during storms, J. Geophys. Res., 112, A10220, doi:10.1029/2007JA012368.

Li, W., et al. (2009), Global distribution of whistler-mode chorus waves observed on the THEMIS spacecraft, Geophys. Res. Lett., 36, L09104, doi:10.1029/2009GL037595.

Li, W., Q. Ma, R. M. Thorne, J. Bortnik, C. A. Kletzing, W. S. Kurth, G. B. Hospodarsky, and Y. Nishimura (2015), Statistical properties of plasmaspheric hiss derived from Van Allen Probes data and their effects on radiation belt electron dynamics, J. Geophys. Res. Space Physics, 120, 3393–3405, doi:10.1002/2015JA021048.

Liu, N., et al. (2017), Simultaneous disappearances of plasmaspheric hiss, exohiss, and chorus waves triggered by a sudden decrease in solar wind dynamic pressure, Geophys. Res. Lett., 44, 52–61, doi:10.1002/2016GL071987.

Lorentzen, K. R., J. B. Blake, U. S. Inan, and J. Bortnik (2001), Observations of relativistic electron microbursts in association with VLF chorus, J. Geophys. Res., 106(A4), 6017–6027, doi:10.1029/2000JA003018.

Lyons, L. R., and R. M. Thorne (1973), Equilibrium structure of radiation belt electrons, J. Geophys. Res., 78(13), 2142–2149, doi:10.1029/JA078i013p02142.

Ma, Q., et al. (2016), Characteristic energy range of electron scattering due to plasmaspheric hiss, J. Geophys. Res. Space Physics, 121, 11, 737–11, 749, doi:10.1002/2016JA023311.

Mauk, B. H., N. J. Fox, S. G. Kanekal, R. L. Kessel, D. G. Sibeck, and A. Ukhorskiy (2013), Science Objectives and Rationale for the Radiation Belt Storm Probes Mission, Space Sci Rev, 179(1), 3–27, doi:10.1007/s11214-012-9908-y.

McFadden, J. P., C. W. Carlson, D. Larson, J. Bonnell, F. Mozer, V. Angelopoulos, K.-H. Glassmeier, and U. Auster (2008), THEMIS ESA first science results and performance issues, Space Sci. Rev., 141, 477–508, doi:10.1007/s11214-008-9433-1.

Meredith, N. P., R. B. Horne, and R. R. Anderson (2001), Substorm dependence of chorus amplitudes: Implications for the acceleration of electrons to relativistic energies, J. Geophys. Res., 106(A7), 13,165–13,178, doi:10.1029/2000JA900156.

Meredith, N. P., R. B. Horne, R. H. A. Iles, R. M. Thorne, D. Heynderickx, and R. R. Anderson (2002), Outer zone relativistic electron acceleration associated with substorm - enhanced whistler mode chorus, J. Geophys. Res., 107(A7), 1144, doi:10.1029/2001JA900146.

Meredith, N. P., R. B. Horne, R. M. Thorne, and R. R. Anderson (2003), Favored regions for chorus-driven electron acceleration to relativistic energies in the Earth's outer radiation belt, Geophys. Res. Lett., 30(16),1871, doi:10.1029/2003GL017698.

Meredith, N. P., R. B. Horne, R. M. Thorne, D. Summers, and R. R. Anderson (2004), Substorm dependence of plasmaspheric hiss, J. Geophys. Res., 109, A06209, doi:10.1029/2004JA010387.

Meredith, N. P., R. B. Horne, S. A. Glauert, R. M. Thorne, D. Summers, J. M. Albert, and R. R. Anderson (2006), Energetic outer zone electron loss timescales during low geomagnetic activity, J. Geophys. Res., 111, A05212, doi:10.1029/2005JA011516.

Meredith, N. P., R. B. Horne, S. A. Glauert, and R. R. Anderson (2007), Slot region electron loss timescales due to plasmaspheric hiss and lightning-generated whistlers, J. Geophys. Res., 112, A08214, doi:10.1029/2007JA012413.

Meredith, N. P., R. B. Horne, S. A. Glauert, D. N. Baker, S. G. Kanekal, and J. M. Albert (2009), Relativistic electron loss timescales in the slot region, J. Geophys. Res., 114, A03222, doi:10.1029/2008JA013889.

Miyoshi, Y., A. Morioka, R. Kataoka, Y. Kasahara, and T. Mukai (2007), Evolution of the outer radiation belt during the November 1993 storms driven by corotating interaction regions, J. Geophys. Res., 112, A05210, doi:10.1029/2006JA012148.

Ni, B., et al. (2014), Resonant scattering of energetic electrons by unusual low-frequency hiss, Geophys. Res. Lett., 41, 1854–1861, doi:10.1002/2014GL059389.

Reeves, G. D., et al. (2013), Electron acceleration in the heart of the Van Allen radiation belts, Science, 341(6149), 991–994, doi:10.1126/science.1237743.

Santolík, O., D. A. Gurnett, J. S. Pickett, M. Parrot, and N. Cornilleau-Wehrlin (2003), Spatio-temporal structure of storm-time chorus, J. Geophys. Res., 108(A7), 1278, doi:10.1029/2002JA009791.

Shprits, Y. Y., D. Subbotin, and B. Ni (2009), Evolution of electron fluxes in the outer radiation belt computed with the VERB code, J. Geophys. Res., 114, A11209, doi:10.1029/2008JA013784.

Spasojevic, M., Y. Y. Shprits, and K. Orlova (2015), Global empirical models of plasmaspheric hiss using Van Allen Probes, J. Geophys. Res. Space Physics, 120, 10,370–10,383, doi:10.1002/2015JA021803.

Spence, H., et al. (2013), Science goals and overview of the Radiation Belt Storm Probes (RBSP) Energetic Particle, Composition, and Thermal Plasma (ECT) suite on NASA's Van Allen Probes mission, Space Sci. Rev., 179(1-4), 311–336, doi:10.1007/s11214-013-0007-5.

Su, Z., et al. (2015), Disappearance of plasmaspheric hiss following interplanetary shock, Geophys. Res. Lett., 42, 3129–3140, doi:10.1002/2015GL063906.

Summers, D., B. Ni, N. P. Meredith, R. B. Horne, R. M. Thorne, M. B. Moldwin, and R. R. Anderson (2008), Electron scattering by whistler-mode elf hiss in plasmaspheric plumes, J. Geophys. Res., 113, A04219, doi:10.1029/2007JA012678.

Tao, X., Q. Lu, S. Wang, and L. Dai (2014), Effects of magnetic field configuration on the day-night asymmetry of chorus occurrence rate: A numerical study, Geophys. Res. Lett., 41, 6577–6582, doi:10.1002/2014GL061493.

Thorne, R. M., E. J. Smith, R. K. Burton, and R. E. Holzer (1973), Plasmaspheric hiss, J. Geophys. Res., 78, 1581–1596, doi:10.1029/JA078i010p01581.

Thorne, R. M., T. P. O'Brien, Y. Y. Shprits, D. Summers, and R. B. Horne (2005), Timescale for MeV electron microburst loss during geomagnetic storms, J. Geophys. Res., 110, A09202, doi:10.1029/2004JA010882.

Thorne, R. M., et al. (2013a), Rapid local acceleration of relativistic radiation-belt electrons by magnetospheric chorus, Nature, 504, 411–414, doi:10.1038/nature12889.

Thorne, R. M., et al. (2013b), Evolution and slow decay of an unusual narrow ring of relativistic electrons near L ~ 3.2 following the September 2012 magnetic storm, Geophys. Res. Lett., 40, 3507–3511, doi:10.1002/grl.50627.

Tsurutani, B. T., and E. J. Smith (1974), Postmidnight chorus: A substorm phenomenon

Tsurutani, B. T., and E. J. Smith (1974), Postmidnight chorus: A substorm phenomenon, J. Geophys. Res., 79(1), 118–127, doi:10.1029/JA079i001p00118.

Tsurutani, B. T., and E. J. Smith (1977), Two types of magnetospheric ELF chorus and their substorm dependences, J. Geophys. Res., 82(32), 5112–5128, doi:10.1029/JA082i032p05112.

Tsurutani, B. T., B. J. Falkowski, J. S. Pickett, O. Santolik, and G. S. Lakhina (2015), Plasmaspheric hiss properties: Observations from Polar, J. Geophys. Res. Space Physics, 120, 414–431, doi:10.1002/2014JA020518.

Tsyganenko, N. A. (1989), A magnetospheric magnetic field model with a warped tail current sheet, Planet. Space Sci., 37, 5–20.

Wang, C., J. B. Liu, H. Li, Z. H. Huang, J. D. Richardson, and J. R. Kan (2009), Geospace magnetic field responses to interplanetary shocks, J. Geophys. Res., 114, A05211, doi:10.1029/2008JA013794.

Wygant, J. R., et al. (2013), The electric field and waves instruments on the radiation belt storm probes mission, Space Sci. Rev., 179(1-4), 183–220, doi:10.1007/s11214-013-0013-7.

Yue, C., Q.-G. Zong, and Y. F. Wang (2009), Response of the magnetic field and plasmas at the geosynchronous orbit to interplanetary shock, Chin. Sci. Bull., 54, 4241–4252, doi:10.1007/s11434-009-0649-6.

Yue, C., Q.-G. Zong, H. Zhang, Y. F. Wang, C. J. Yuan, Z. Y. Pu, S. Y. Fu, A. T. Y. Lui, B. Yang, and C. R. Wang (2010), Geomagnetic activities triggered by interplanetary shocks, J. Geophys. Res., 115, A00I05, doi:10.1029/2010JA015356.

Yue, C., Q. Zong, Y. Wang, I. I. Vogiatzis, Z. Pu, S. Fu, and Q. Shi (2011a), Inner magnetosphere plasma characteristics in response to interplanetary shock impacts, J. Geophys. Res., 116, A11206, doi:10.1029/2011JA016736.

Yue, C., and Q. Zong (2011b), Solar wind parameters and geomagnetic indices for four different interplanetary shock/ICME structures, J. Geophys. Res., 116, A12201, doi:10.1029/2011JA017013.

Yue, C., Y. Nishimura, L. R. Lyons, V. Angelopoulos, E. F. Donovan, Q. Shi, Z. Yao, and J. W. Bonnell (2013), Coordinated THEMIS spacecraft and all-sky imager observations of interplanetary shock effects on plasma sheet flow bursts, poleward boundary intensifications, and streamers, J. Geophys. Res. Space Physics, 118, 3346–3356, doi:10.1002/jgra.50372.

Yue, C., et al. (2016a), Rapid enhancement of low-energy (<100 eV) ion flux in response to interplanetary shocks based on two Van Allen Probes case studies: Implications for source regions and heating mechanisms, J. Geophys. Res. Space Physics, 121, 6430–6443, doi:10.1002/2016JA022808.

Yue, C., X. An, J. Bortnik, Q. Ma, W. Li, R. M. Thorne, G. D. Reeves, M. Gkioulidou, D. G. Mitchell, and C. A. Kletzing (2016b), The relationship between the macroscopic state of electrons and the properties of chorus waves observed by the Van Allen Probes, Geophys. Res. Lett., 43, 7804–7812, doi:10.1002/2016GL070084.

Zhou, C., et al. (2015), Excitation of dayside chorus waves due to magnetic field line compression in response to interplanetary shocks, J. Geophys. Res. Space Physics, 120, 8327–8338, doi:10.1002/2015JA021530.

Figure Captions:

Figure 1. (a) An IP shock observed by the THEMIS-C spacecraft at 16:57 UT at (-21.2, 57.5, -1.7) R_E in solar wind on 7 June 2014. The top panel shows magnetic field magnitude in black and the X-component of solar wind velocity in GSE coordinate in red. The bottom panel shows ion density in black and dynamic pressure in red; (b) The variations of geomagnetic indices during the same time interval as in Figure 1a. The

vertical dashed line marks the shock arrival time at ground observation; (c) and (d) are the wave and electron measurements by Van Allen Probes A and B, respectively. The panels from top to bottom are the electric spectral density in the HFR channel, electric and magnetic field power spectral densities in the WFR channel, and the omni-directional electron energy flux from 0.1 to 20 keV. The vertical dashed line marks the shock arrival time.

Figure 2. (a) An IP shock observed by the THEMIS-C spacecraft at 17:04 UT at (-8.3, 60.7, -2.8) R_E in solar wind on 7 February 2014. The first panel shows magnetic field magnitude in black and the X-component of solar wind velocity in GSE coordinates in red. The second panel shows ion density in black and dynamic pressure in red. The bottom panel shows the variations of AE index in black and symH in red. (b) The magnetic field power spectral density in the parallel and perpendicular directions observed by THEMIS-D. The vertical dashed line marks the IP shock arrival time. (c) and (d) are the wave and electron measurements made by Van Allen Probes A and B, respectively. The panels from top to bottom are the electric spectral density in the HFR channel, electric and magnetic field power spectral density in the WFR channel, and the omni-directional electron energy flux from 0.1 to 20 keV. The vertical dashed line marks the shock arrival time.

Figure 3. The global distribution of the whistler mode chorus and plasmaspheric hiss wave responses to IP shocks observed by Van Allen Probes and THEMIS satellites. (a) Distribution in the X-Y plane in SM coordinates. The cross sign represents the locations

of Van Allen Probes and the diamond sign represents the locations of THEMIS satellites around the IP shock arrival time; (b) and (c) Event distributions as function of MLTs (b) and MLAT (c). Blue color represents hiss wave reduction/disappearance; Red color represents hiss wave intensification/excitation; Black represents chorus wave intensification/excitation.

Figure 4. Illustration of ray tracing in the noon-midnight meridian plane for chorus waves of different wave normal angles (color-coded) launched with a fixed frequency 500 Hz at L=7 at the magnetic equator during quiet (Kp=1, top panel) and disturbed (Kp=6, bottom panel) conditions based on T89 magnetic field model. The plasmapause location is at L_{pp}=5.5.

Figures.

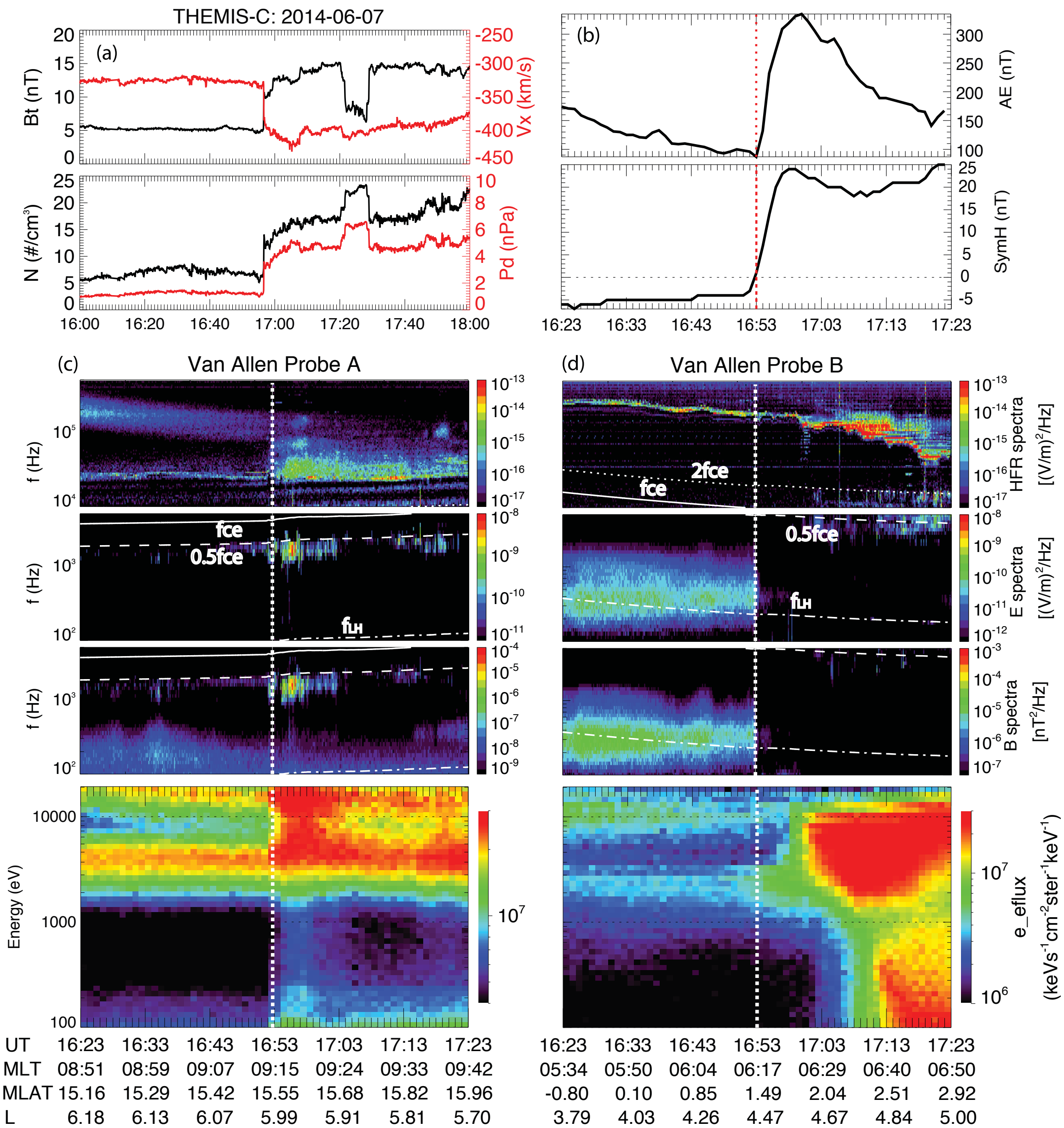

Figure 1. (a) An IP shock observed by the THEMIS-C spacecraft at 16:57 UT at (-21.2, 57.5, -1.7) R_E in solar wind on 7 June 2014. The top panel shows magnetic field magnitude in black and the X-component of solar wind velocity in GSE coordinate in red. The bottom panel shows ion density in black and dynamic pressure in red; (b) The variations of geomagnetic indices during the same time interval as in Figure 1a. The vertical dashed line marks the shock arrival time at ground observation; (c) and (d) are

the wave and electron measurements by Van Allen Probes A and B, respectively. The panels from top to bottom are the electric spectral density in the HFR channel, electric and magnetic field power spectral densities in the WFR channel, and the omni-directional electron energy flux from 0.1 to 20 keV. The vertical dashed line marks the shock arrival time.

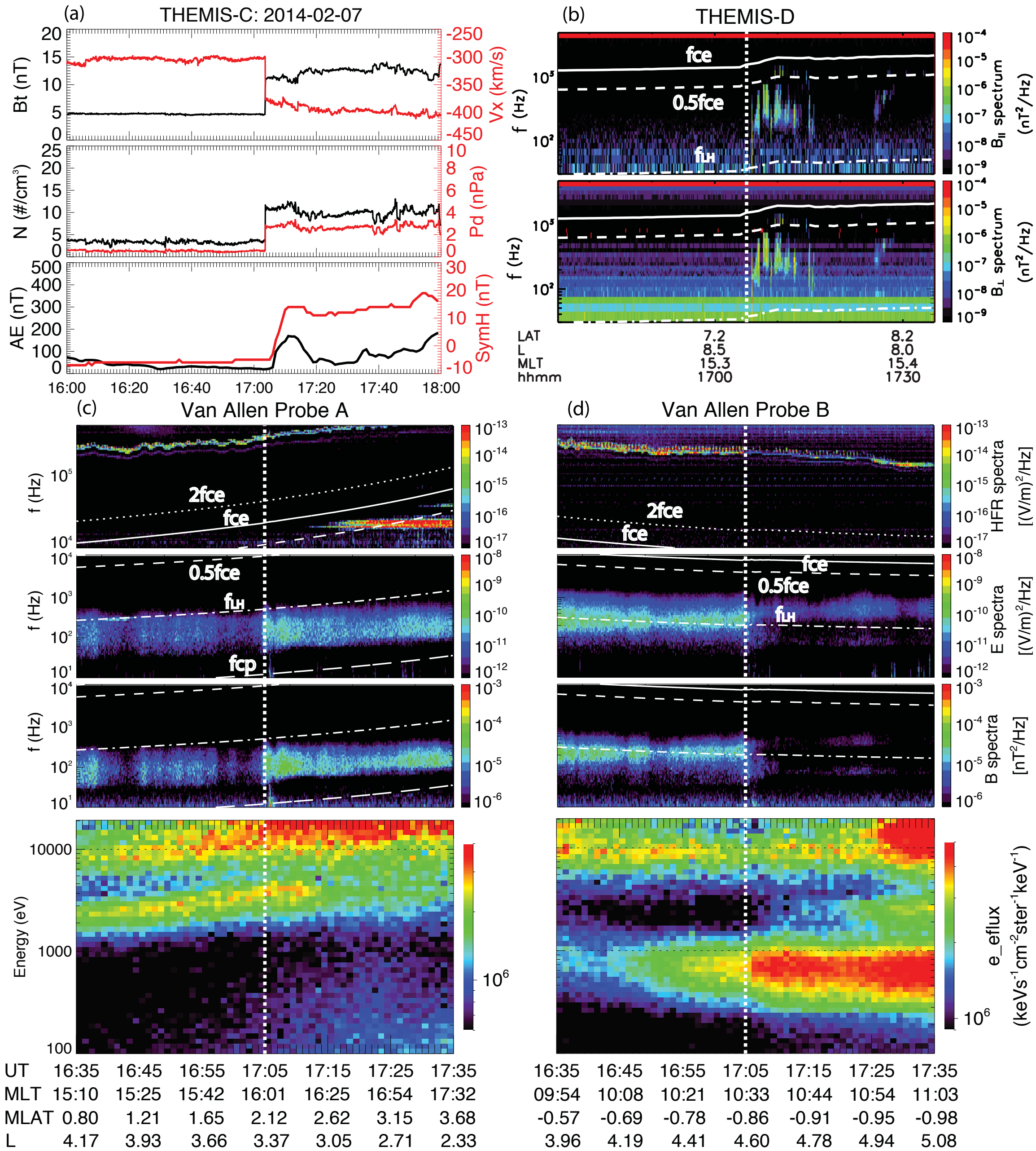

Figure 2. (a) An IP shock observed by the THEMIS-C spacecraft at 17:04 UT at (-8.3, 60.7, -2.8) R_E in solar wind on 7 February 2014. The first panel shows magnetic field magnitude in black and the X-component of solar wind velocity in GSE coordinates in red. The second panel shows ion density in black and dynamic pressure in red. The bottom panel shows the variations of AE index in black and symH in red. (b) The

magnetic field power spectral density in the parallel and perpendicular directions observed by THEMIS-D. The vertical dashed line marks the IP shock arrival time. (c) and (d) are the wave and electron measurements made by Van Allen Probes A and B, respectively. The panels from top to bottom are the electric spectral density in the HFR channel, electric and magnetic field power spectral density in the WFR channel, and the omni-directional electron energy flux from 0.1 to 20 keV. The vertical dashed line marks the shock arrival time.

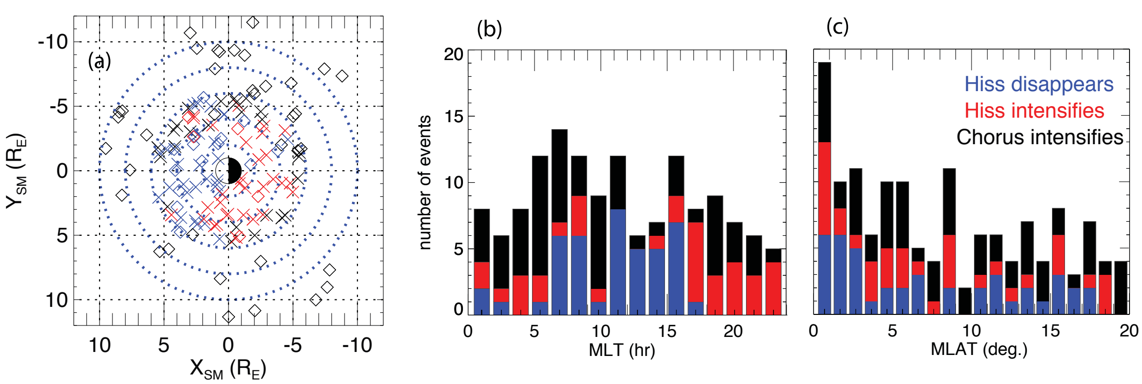

Figure 3. The global distribution of the chorus and hiss wave responses to IP shocks observed by Van Allen Probes and THEMIS satellites. (a) Distribution in the X-Y plane in SM coordinates. The cross sign represents the locations of Van Allen Probes and the diamond sign represents the locations of THEMIS satellites around the IP shock arrival time; (b) and (c) Event distributions as function of MLTs (b) and MLAT (c). Blue color represents hiss wave reduction/disappearance; Red color represents hiss wave intensification/excitation; Black represents chorus wave intensification/excitation.

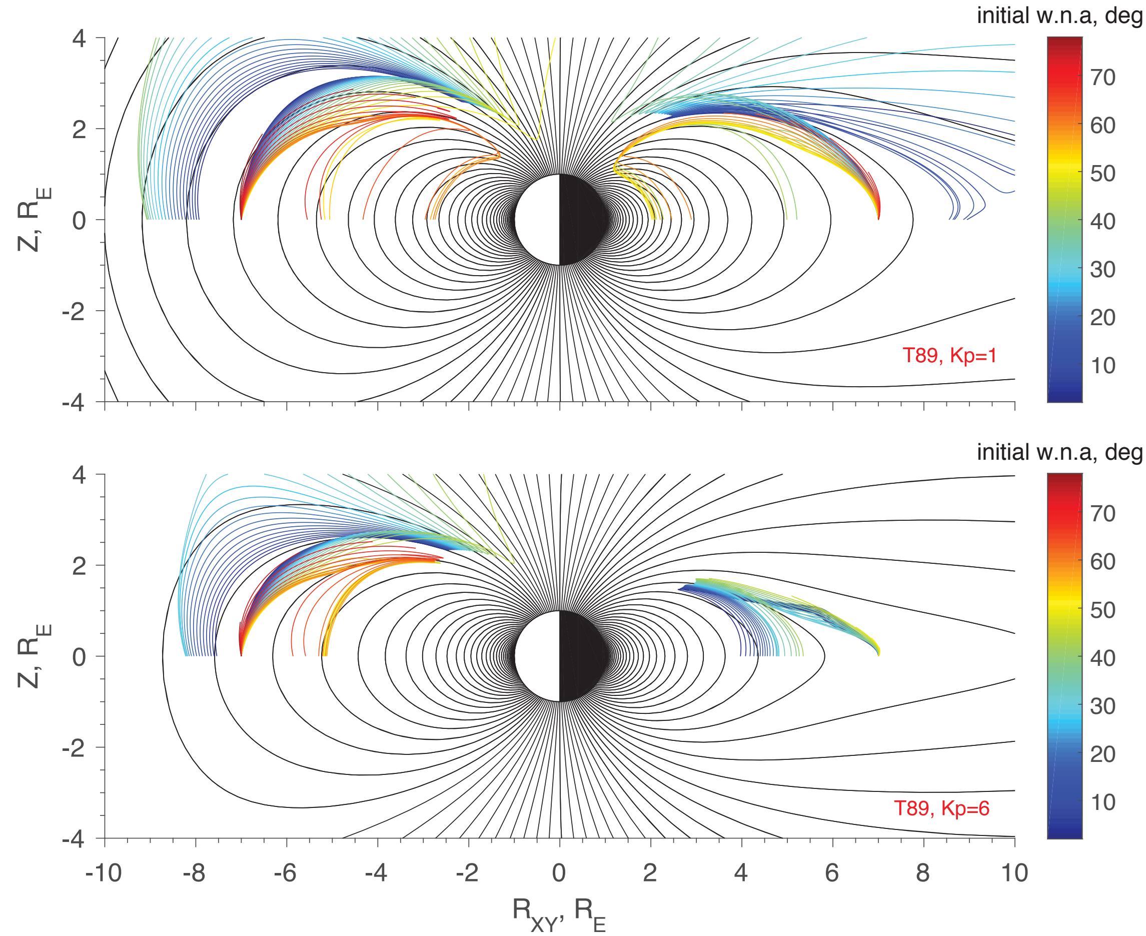

Figure 4. Illustration of ray tracing in the noon-midnight meridian plane for chorus waves of different wave normal angles (color-coded) launched with a fixed frequency 500 Hz at L=7 at the magnetic equator during quiet (Kp=1, top panel) and disturbed (Kp=6, bottom panel) conditions based on T89 magnetic field model. The plasmapause location is at L_{pp}=5.5.